CSI (COMITÉ DE SUIVI INDIVIDUEL) REPORT

Comparative assessment of the speed and accuracy performances of numerical solvers for complex naval applications

DESCAMPS THÉO

Supervisor : Prof. LE TOUZÉ DAVID
Co-supervisor : BOUSCASSE BENJAMIN
Co-supervisor : GENTAZ LIONEL

1st April 2019 — 30th September 2020

Chapter 1

Overview

1.1 Introduction

Seakeeping, including the evaluation of added resistance, is today a major concern for engineering offices or shipyards designing ships as well as for classification companies because the prediction of motions in waves and additional resistance due to waves are key elements in the evaluation of ship performance, the reduction of greenhouse gas emissions, the security of equipment and personnel.

In this context, the development of efficient numerical methods is necessary. First numerical solutions based on potential theory have been developed a long time ago being proposed from the 60's. These methods are based on frequency domain or time domain. Nonlinearities in the hull and free surface boundary conditions are treated at different levels from linear level very commonly used for reducing the computational effort up to weak-scatter methods (body exact method, free surface boundary conditions applied on the incident nonlinear wave shape) or even fully nonlinear level.

This Ph.D. is part of the research conducted by the Bureau Veritas MarineOffshore and Ecole Centrale Nantes. The objective of the present Ph.D. is to study the phenomena involved in the wave added resistance, to develop the solvers and methodologies to improve computational time and accuracy with regards to wave added resistance, and to perform validations and applications on hull form optimisation.

These objectives entail several topics. The first step is to get an accurate sea state numerical model. This step was partly achieve before the start of this Ph.D. by Li (2018), Choi (2019) and Kim et al. (2018) to name but a few. Existing solutions had to be improved and deepen in order to properly simulate most common ocean see states in which ships navigate at there operating speed. The second step is to properly simulate ship motions with all degrees of freedom, forward speed and several kind of appendages.

This document provides an overview of the work realised during the first part of the past year.

1.2 Mathematical model

This section is a quick overview of the different mathematical model involved in the summarized studies. Before any numerical implementation the choice of the mathematical

model is obviously crucial in order to model accurately the phenomena that cannot be neglected in the simulation. The validity of a model is directly impact by the terms that are neglected or not.

1.2.1 Navier stokes

The general Navier stokes equations modelling a non compressible Newtonian flow can be written as follow.

$$\nabla \bullet \mathbf{u} = 0 \tag{1.1a}$$

$$\rho \frac{d\mathbf{u}}{dt} = \rho \boldsymbol{g} - \nabla P + \mu \Delta \mathbf{u} \tag{1.1b}$$

Solving those equations without any simplification is called the Direct Numerical Navier Stokes method (DNS). Whatever the numerical method employed, as no simplification are down by this model (compared to the other ones), in naval application, the computation cost will always be large.

1.2.2 Reynolds Average Navier Stokes

For naval application, now a day, the Navier Stokes equations are often used in a transformed form called Reynolds Average Navier Stokes Equations (RANSE). This model consist in using the Reynolds statistical decomposition and modelling the average turbulence effects introducing the turbulent viscosity ν_{t} and the turbulent kinetic energy k. Those variables model the small scale phenomena related to velocity fluctuations.

The two-phase incompressible RANS Equations can be written in their conservative form (Eq. (1.2a) and Eq. (1.2b)).

$$\nabla \bullet \mathbf{u} = 0 \tag{1.2a}$$

$$\frac{\partial(\rho \mathbf{u})}{\partial t} + \nabla \bullet (\rho \mathbf{u}\mathbf{u}) - \nabla \bullet (\mu_{\mathrm{eff}}(\nabla \mathbf{u} + \nabla \mathbf{u}^{\mathrm{T}})) = -\nabla p_{\mathrm{d}} + gz\nabla\rho \tag{1.2b}$$

Where $\mathbf{u}$ is the velocity vector field, ρ is the density of fluid, p_{d} is the "dynamic pressure" field defined as $p_{\mathrm{d}} = p + \frac{2}{3}\rho k + \rho g z$, p is the total pressure, g is the gravitational acceleration scalar, z is the vertical coordinate in the reference frame and μ_{eff} is the effective dynamic viscosity defined as $\mu_{\mathrm{eff}} = \mu + \rho \nu_{\mathrm{t}}$, with μ the fluid dynamic viscosity.

These equations are convenient for naval application because they model unsteady flow taking into account inertial, volumic, pressure and viscous forces. The small scale turbulent phenomena are only considered through their average influence so RANSE resolution has a significantly smaller computational cost than DNS.

An alternative model called Large Eddy Simulation (LES) is sometimes used in order to model with accuracy some turbulent phenomena. This is occasionally used in naval application in order to simulate massively separated flows. As the LES simulation imposes more refined

mesh than RANSE near to the bodies, the Detached-Eddy Simulation (DES) method can be used. It combines LES method far from the body and RANSE method near to it (Spalart, 2009). It is employed for instance for accurate ship airwakes computation (Forrest and Owen, 2010). This method will not be considered during this Ph.D.

1.2.3 Euler

At large Reynolds number, the viscosity term in the RANS equations can be neglected. This results in considering an inviscid flow satisfying the Euler equations.

$$\nabla \bullet \mathbf{u} = 0 \tag{1.3a}$$

$$\frac{\partial(\rho \mathbf{u})}{\partial t} + \nabla \bullet (\rho \mathbf{u}\mathbf{u}) = -\nabla p + \rho\, \mathbf{g} \tag{1.3b}$$

This mathematical model itself is unusually used for naval application. However it is a key point of the Spectral Wave Explicit Navier Stokes Equations (SWENSE) formulation described in the following.

1.2.4 Potential flow

The hypothesis of non rotational flow implies the existence of a potential field Φ such as $\mathbf{u} = \nabla\Phi$. Adding this hypothesis to the Euler equations results in potential flow equations:

$$\Delta\Phi = 0 \tag{1.4a}$$

$$\frac{\partial \phi}{\partial t} + \frac{\mathbf{u}^2}{2} + gz + \frac{P}{\rho} = F(t) \tag{1.4b}$$

Numerically, these equations allow to use some accurate integration methods requiring significantly small computational cost. The potential flow theory is commonly convenient for unbreaking wave simulations without body because of viscous effects that can be neglected. The High Order Spectral (HOS) method detailed in the following lies on this mathematical model. Beside, as potential flow theory allows small computational cost, in the past many naval applications were studied using this model and it is still employed today for high Reynolds number flows simulations with weak viscosity effect as uncounted in some seakeeping applications.

1.2.5 SWENSE

The Spectral Wave Explicit Navier Stokes (SWENS) method (Ferrant et al., 2003) was developed in the LHEEA in order to acculturated simulate wave-structure iteration with complex sea states. The main idea is to solve separately the ”incident fields” mainly corresponding to the wave filed and the ”complementary fields” (Figure. 1.1). This complementary fields is defined as the difference of the total field and the incident one so it takes evidently into account the diffracted fields but also all the ”corrections” implies by the

chosen incident field. For example, it encompasses phenomena neglected in the incident fields and some non physic numerical considerations related to the incident field solving method.

Mathematically, the SWENS method is based on the hypothesis that the incident fields verify the Euler equations and the total field the RANS equations. The governing equation of the complementary field are called Spectral Wave Explicit Navier Stokes equations (SWENSE)

With SWENSE, only the complementary part is solve using a CFD solver. The incident fields are already know before the simulation and appear as a forcing terms during the computation. The most accurate method to get these initial fields is to compute them using potential flow theory. Those methods are discussed in the following.

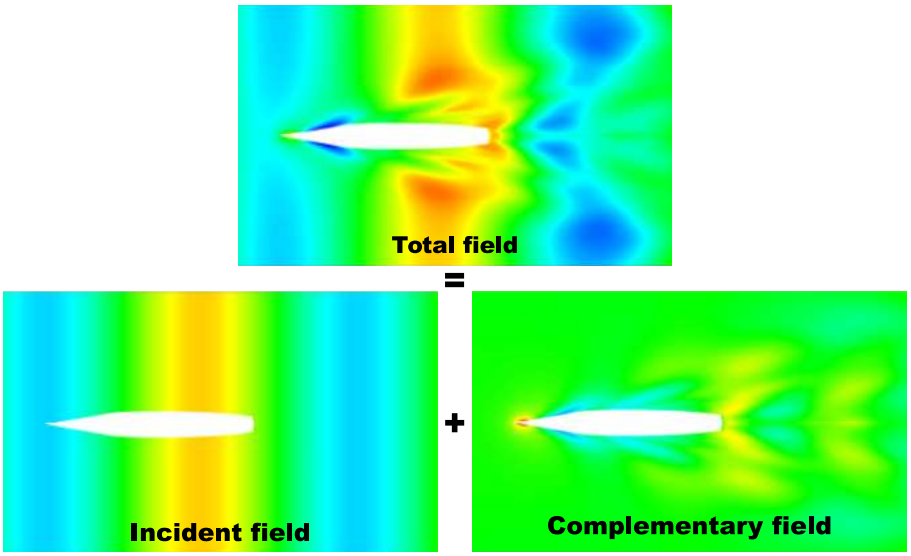

Figure 1.1: The SWENSE method decomposes the total field into an incident part and a complementary part

Assuming the incident part of the flow is inviscid and satisfying the incompressible flow condition, the incident velocity ($\mathbf{u}_\mathrm{I}$) and the incident pressure (p_I) follow the continuity equation (Eq. (1.5a)) and the Euler equation (Eq. (1.5b)). The Euler equation is valid only for single phase flow where $\rho = \rho_\mathrm{water}$.

$$\nabla \bullet \mathbf{u}_\mathrm{I} = 0 \tag{1.5a}$$

$$\frac{\partial(\rho_\mathrm{water}\mathbf{u}_\mathrm{I})}{\partial t} + \nabla \bullet (\rho_\mathrm{water}\mathbf{u}_\mathrm{I}\mathbf{u}_\mathrm{I}) = -\nabla p_\mathrm{I} + \rho_\mathrm{water}\,\mathbf{g} \tag{1.5b}$$

Since this incident wave field is not computed by the SWENSE solver some advantages are expected. Firstly, only the complementary field has to be damped in the outer region, this is a field of smaller magnitude easier to absorb than the total field including incident waves. Secondly, the mesh has to be designed for the complementary field and this gives potential for reducing the cells number by using a coarser resolution in the far field and consequently reducing the computation time (typically by using similar meshes as for calm water studies).

1.3 foamStar and foamStar-SWENSE

The studies summarized in this document, are all carried out using the internally developed solver *foamStar* based on OpenFOAM open-source library and its SWENSE implementation (*foamStar-SWENSE*). For both implementations the turbulent flow is solved in a similar way. RANS equations are applied to a two-phase viscous, incompressible flow. Two-phase approach is modeled by a VOF method (Hirt and Nichols, 1981). The discretization of equations is managed with an unstructured polyhedral finite volume method. Both solvers couples pressure and velocity using PISO algorithm (inner iteration) and the SIMPLE iteration couples the VOF with the velocity. This combination of PISO and SIMPLE is PIMPLE iteration (outer iteration). Also, the non-orthogonal correction in Laplacian operator is applied to minimize the error from the non-orthogonality (Jasak, 1996a; Moukalled et al., 2016). In this work, the turbulent model used is $k-\omega$ SST and viscous layer is modelled using wall functions.

1.3.1 Wave generation

In *foamStar* the wave generation is done using potential flow models. The regular waves are generated using stream-function wave theory (Rienecker and Fenton, 1981) and the irregular sea states are generated using the High-Order Spectral (HOS) method (West et al., 1987; Dommermuth and Yue, 1987). In this method, the nonlinear free surface boundary conditions are written in terms of the two surface quantities of interest, namely the free surface elevation $\eta(\mathbf{x},t)$ and the free surface velocity potential $\widetilde{\phi}(\mathbf{x},t) = \phi(\mathbf{x}, z = \eta(\mathbf{x},t), t)$

$$\frac{\partial \eta}{\partial t} = \left(1 + |\nabla \eta|^2\right) W - \nabla \widetilde{\phi}.\nabla \eta \tag{1.6}$$

$$\frac{\partial \widetilde{\phi}}{\partial t} = -g\eta - \frac{1}{2}\left|\nabla \widetilde{\phi}\right|^2 + \frac{1}{2}\left(1 + |\nabla \eta|^2\right) W^2 \tag{1.7}$$

These boundary conditions are expressed at the exact free surface location $z = \eta(\mathbf{x},t)$ and enable the time-marching of the two unknowns (η and $\widetilde{\phi}$) once the free surface vertical velocity $W = \left(\frac{\partial \phi}{\partial z}\right)(\mathbf{x}, z = \eta(\mathbf{x},t), t)$ is evaluated. This is achieved through the HOS procedure that performs a series expansion in wave steepness ε up to the so-called HOS nonlinear order M together with a Taylor series expansion around $z = 0$ in order to allow an iterative and efficient solution of the problem.

The open-source code *HOS-ocean* is implemented for the solution of the wave propagation problem and we refer to (Ducrozet et al., 2016) for more details. The coupling procedure with the CFD model is achieved through the wrapper open-source program *Grid2Grid* that enables to recompute the incident wave field at any position and time, see Choi et al. (2017).

1.3.2 Relaxation scheme

Ensuring a sufficient quality of the wave generation and propagation with a viscous flow approach is a crucial point for computing accurate body responses in waves. This is particularly true in irregular waves simulations for which evaluating long-term statistical quantities might require thousands of waves interacting with the ship.

Waves are quite often generated in numerical domain by forcing wave velocities in a specific plane or volume usually on the side on the domain. Consequently fine grids are required to propagate waves from outer boundaries to the ship without noticeable damping. 50 to 100 nodes per wavelength are typically needed on the free surface for regular waves propagation (Li (2018) and Choi (2019)). Moreover, successive reflections of incident waves between ship and outer boundaries can reduce the usable duration of outputs as it happens in physical wave tanks. To overcome these difficulties different methods can be found in the literature: internal wave generators where sources or dipoles below the free surface generate incident waves (Larsen and Dancy, 1983), relaxation zones which are implemented near outer boundaries (where generation is done) to absorb reflected waves.

The relaxation zone approach is used to efficiently generate and absorb the waves in the computational domain (Jacobsen et al., 2012; Li et al., 2019). After the flow field (χ^{CFD}) is obtained from the governing equation, *foamStar* update the quantity χ using explicit relaxation scheme which blends the computed solution with target flow field (χ^{Target}) in the relaxation zones.

$$\chi = (1-w)\chi^{CFD} + w\chi^{\text{Target}} \tag{1.8}$$

Eq. (1.8) shows the explicit blending of the flow field, where w is a weight function varying from 0 to 1 in the relaxation zone. The relaxation zone relax the VOF field and the velocity field.

In the case of *foamStar-SWENSE*, the relaxation zone relax only the complementary flow velocity, and the natural target function is zero.

$$\mathbf{u}_{\text{C}} = (1-w)\mathbf{u}_{\text{C}}^{CFD} \tag{1.9}$$

Eq. (1.10) is the weight function used in this study. It is an exponential weight function, and it is defined in the normalized coordinate ξ.

$$w(\xi) = \frac{e^{\xi_{relax}^{3.5}} - 1}{e-1}, \quad \xi \in [0,1] \tag{1.10}$$

1.3.3 SWENSE implementation

Incident field treatment for the air phase for SWENSE

The SWENSE method requires the evaluation of incident flow above the incident wave free surface in order to perform the subtraction leading to the system of equations Eq. (1.14) and Eq. (1.15). The numerical performances of the SWENSE method (accuracy, efficiency, robustness) rely on an extrapolation satisfying specific features:

- continuity of the fields through the incident free surface elevation;
- Incompressible mono-fluid incident flow.

The incident wave models presented in previous section actually allow an extrapolation of the fields for $z > \eta_I$ satisfying the two criteria. However, the hyperbolic characteristics of the wave components in the vertical direction possibly generate very large velocity and pressure fields. It might cause undesirable numerical instability, especially in the air zone. Li (2018) tested to limit the magnitude of the incident fields in the air. The extension was consequently operated up to a given stretching limit and the value at the limit was imposed above it. However, due to the large gradients at the stretching limit, numerical instabilities may develop..

To overcome the issue, Choi (2019) used a cubic interpolation to smooth the incident wave field in the air phase. Figure 1.2 illustrates the concept of the wave field interpolation. The wave field is extended in the buffer zone thanks to the spectral representation of the quantities. Then, the coefficients of the cubic polynomial in the interpolation zone are determined explicitly using the Neumann and Dirichlet boundary conditions at the boundaries of interpolation zone. The vertical gradient between wind zone and interpolation zone is set to zero, and the vertical gradient between water zone and interpolation zone is calculated numerically. The length of interpolation zone is $h_{\text{thickness}} = 2H$ and buffer zone is $h_{\text{ref}} = 0.02H$, where H is the wave height.

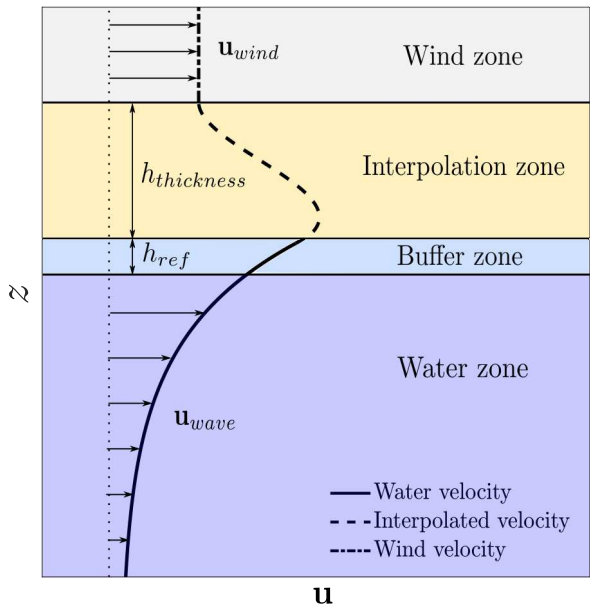

Figure 1.2: Schematic illustration on the incident wave field interpolation over the free surface

SWENSE VOF

The SWENSE formulation subtracts the incident Euler equation (Eq. (1.5b)) from the original RANSE equation (Eq. (1.2b)). This was shown to be a difficulty in two-phase flow by Li (2018). Thanks to the spectral methods, the incident wave fields can be extended in the entire computational domain directly. From this extension, Euler equation (Eq. (1.5b)) is valid in the entire domain. Consequently, subtracting the Eq. (1.5b) from Eq. (1.2b) generates an extra pressure term that cannot be neglected in air and causes stability issues. To solve this issue, (Li, 2018) proposed the modified incident pressure using mixture density

$$p_{\mathrm{I}}^{*} = \rho \frac{p_{\mathrm{I}}}{\rho_{\mathrm{I}}}, \tag{1.11}$$

where p_{I}^{*} is the modified incident pressure, ρ is the density of the considered fluid phase and ρ_{I} is the density of the incident field solution ($\rho_{\mathrm{I}} = \rho_{\mathrm{water}}$). The modified Euler's equation for incident terms reads:

$$\frac{\partial(\rho \mathbf{u}_{\mathrm{I}})}{\partial t} + \nabla\bullet(\rho \mathbf{u}_{\mathrm{I}}\mathbf{u}_{\mathrm{I}}) = -\frac{\nabla p_{\mathrm{I}}^{*}}{\rho} + \frac{p_{\mathrm{I}}}{\rho_{\mathrm{I}}}\frac{\nabla\rho}{\rho} + \rho\mathbf{g} \tag{1.12}$$

Eq. (1.13) presents the wave field decomposition. The VOF field is not decomposed in this formulation and uses the same VOF convection equation to the classical two-phase flow solver.

$$\begin{aligned} \mathbf{u} &= \mathbf{u}_{\mathrm{I}} + \mathbf{u}_{\mathrm{C}} \\ p &= p_{\mathrm{I}}^{*} + p_{\mathrm{C}} \end{aligned} \tag{1.13}$$

Then, the subtraction of the incident flow equations from the original RANSE equation yields to a new set of equations for the complementary flow, namely the continuity equation (Eq. (1.14)) and the momentum equation (Eq. (1.15)).

$$\nabla\bullet\mathbf{u}_{\mathrm{C}} = 0 \tag{1.14}$$

$$\frac{\partial(\rho \mathbf{u}_{\mathrm{C}})}{\partial t} + \nabla\bullet(\rho \mathbf{u}\mathbf{u}_{\mathrm{C}}) + \rho\mathbf{u}_{\mathrm{C}}\bullet\nabla\mathbf{u}_{\mathrm{I}} = -\nabla p_{\mathrm{C}} - \frac{p_{\mathrm{I}}}{\rho_{\mathrm{I}}}\nabla\rho + \nabla\bullet(\mu_{\mathrm{eff}}(\nabla\mathbf{u}_{\mathrm{C}} + \nabla\mathbf{u}_{\mathrm{C}}^{\mathrm{T}})) \tag{1.15}$$

Note that the viscous term $\nabla\bullet(\mu_{\mathrm{eff}}(\nabla\mathbf{u}_{\mathrm{I}} + \nabla\mathbf{u}_{\mathrm{I}}^{\mathrm{T}}))$ is considered negligible and it is not included in Eq. (1.15).

1.4 Meshes

Mesh generation is a key point in CFD. Indeed, the development of CFD solver and new computational method such as SWENSE go together with the meshing method. Beside, the numerical errors and uncertainties due to spatial discretization are a crucial aspect of verification procedures. This section discusses those issues and presents the work done over the past year on mesh generation.

1.4.1 Mesh structures

Meshing methods are directly linked to the selected mathematical models and to there numerical implementation.

Surface mesh This type of mesh is specific to the boundary elements methods that only need surface discretisation. That type of simulation is not part of the presented work.

Structured volumic mesh The first type of volumic mesh is the structured mesh. It is characterised by a none topological pattern. This type of mesh eases the spacial high order schemes implementation. It is particularly used with finite different method due to the easiest high order formulation the numerical model allows in contrast with the finite volume method. The CFD solver studied and abandoned at the beginning of this Ph.D. was a finite difference solver that required structured meshes. The principal falling of such a meshing method is the difficulty to manage complex geometry. The quality of the mesh heavily depends on the user skill and cannot really been automatised.

Unstructured volumic mesh The second type of volumic mesh is the unstructured one. This meshing method is now a day the most commonly used in CFD. Unstructured meshes cover all the meshes with arbitrary structure. To generate such meshes is less constraining than creating structured ones but it imposes the use of finite volume method and makes hard the implementation of high order spacial schemes. *foamStar* solver is adapted to unstructured mesh so all the mesh processes discussed in this document are of this type.

During the first half of this Ph.D. several mesh generators were used and compared. It appears that the mesh generation is a significant workload in CFD application. The meshing method is a strong brake to some rigorous analysis of convergence in verification process for the simple reason that changing the mesh density could at least force the change of some parameters of the computation and causes all too often insuperable crashes of the simulation. Consequently, solver management of meshes shortcoming is a key point of CFD and have to be consider cautiously in the research field because of the numerous bias that it could involve.

1.4.2 The mesh quality

Cells Quality and numerical stability

Because of the discretization schemes, the cells shapes are directly linked to the numerical error. Consequently, a convenient mesh would be a mesh for which some cell-shape criteria are respected. An analysis of the numerical error source with finite Volume method is done by Jasak (1996b). Up to now, for naval simulation using foamStar, the two main criteria that seems to impair significantly the simulation are the skewness and the orthogonality.

Beside, the numerical models have some stability requirements in term of Courand number. The time step and the cell size depend of each other to respect those criteria, however, in naval application, because of complex geometry or computational cost, this at first sigh easy to respect Courand number can be a limiting factor.

Mesh related to theoretical models

The second aspect of mesh quality is the relevance to the mathematical and numerical models.

The cell size and shape have to be related to the chosen models. Specific zones in the mesh have to be adapted in order to solve accurately the predominated phenomena. For CFD naval applications, the domain can usually be decomposed into 4 zones:

- the body wall where viscous affect are important;

- the near field where both viscous effect and gravity have to be solve accurately;
- the far field where gravity effects predominate;
- the free surface for which the chosen numerical model implies specific mesh characteristics.

Each zone implies different dominant physical effects or numerical treatment. In order to solve with accuracy every significant phenomena the mesh generation strategy have to follow as far as possible the guidelines related to each zone. During this Ph.D., a distinction between those zones would be a keep point of verification procedures and guidelines realisation.

Chapter 2

Naval applications

In this chapter the objective is to applied the tenet previously exposed to the naval applications at stake in the Ph.D. First, the preliminary subject of the sea state simulation methods is developed. Then, the work done on naval simulations is details. This second point is also the most important one as it aims to meet the final objectives and encompass all the precedent points.

2.1 Sea States simulations

2.1.1 Regular waves propagation

The regular wave propagation using foamStar and foamStar-SWENSE was studied by Li (2018), Choi (2019) and Kim et al. (2018). These works involve the VOF and GFM method and they provide comparison between SWENSE and RANSE regarding to the mesh refinement and numerical schemes. In the present works, the Li (2018) outcomes are considered because of the numerical implementation used.

The objective during this Ph.D. would be to test those recommendations on naval application and occasionally to adapt them. The following study was started in order to take into account the meshing methods used for naval application and to combine them with the 2D waves propagation recommendations. Concerning the meshing method, in the literature it is usual to progressively vertically unrefined the mesh from the free surface to the bottom. Concerning the longitudinal refinement, it is either kept constant all along the mesh, even far from the free surface, or progressively unrefined together with the vertical refinement keeping the same aspect ratio. The figure (2.1) is an example of that type of mesh. The first method lead to large number of cells and it a priori does not seem useful to keep such a refinement far from the free surface and from any body. The second method is more convenient but it is import to keep in mind that the refinement at the free surface have to be strong because of the VOF method. Consequently, the meshes are usually much more refined at the free surface than what the scales of the phenomenon would require just below the free surface. All the more, under the free surface, the scale of the pressure field perturbation in waves is in the order of the wave length and not the wave height. So, under the free surface, to use a vertical refinement related to the wave length could be more convenient than a refinement related to the wave height.

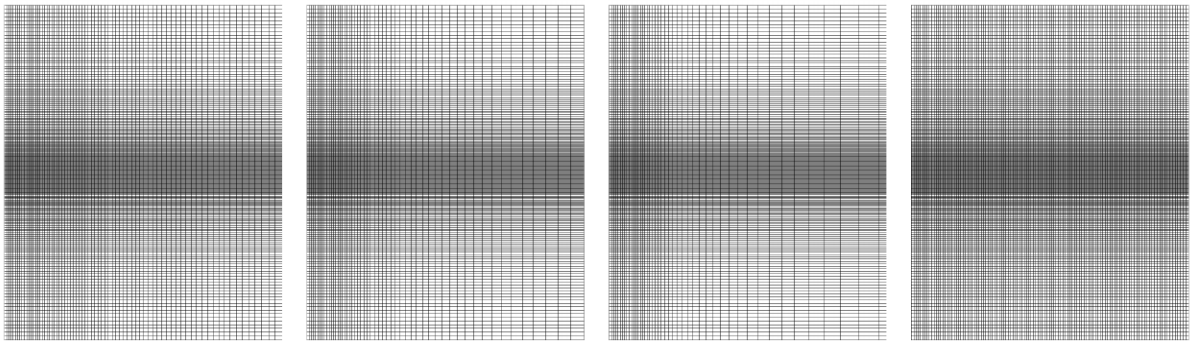

Figure 2.1: Example of meshes used by Choi (2019) for 2D wave propagation studies

study

In this study the accuracy of the wave propagation of 2D regular waves depending on the meshing method is analysed. The solver used for this study is foamStar. The aim of that study is to highlight good mesh generation practices for naval simulation with waves using foamStar and foamStar-SWENSE.

set up

As mentioned before, this work aims naval simulations and not pure wave propagation. Consequently, the set up lies on an other study of scale model container ship in head waves presented in the following (Section. 2.2.2). It implies that a forward speed of $U = 2.017\ m.s^{-1}$ toward is applied.

Waves Among the regular waves taking part into the mentioned naval study, the one with the shortest wavelength is chosen. In fact, the wave damping is all the more a problem for naval simulation as the number of simulated wavelength increase. The characteristics of the wave are: $\lambda = 3.949\ m$, $H = 0.062$.

Mesh The studied mesh are all generated using STAR-CCM+ mesh generator as it is the tool used in the following to generate naval meshes.

The figure (2.2) illustrates the mesh structure. The forward speed is oriented toward the positive X direction and the head waves are generated toward the -X direction. Several refinement zones are defined at the free surface and under. The size of those zones is related to the wave characteristics. The geometry of the mesh is detail in the table (2.1) and the studied refinement are detailed in table (2.2).

The mesh named ”H15L62” is the mesh generated with the ”naive method” only considering a refinement box at the free surface to manage the interface, and keeping the default expansion ration proposed by the mesh generator.

Table 2.1: Zones size in 2D mesh dedicated to regular wave simulation

Zone	**1**	**2**	**3**	**4**
Zmin	$-H$	$-\lambda/4$	$-\lambda/2$	$-\lambda$

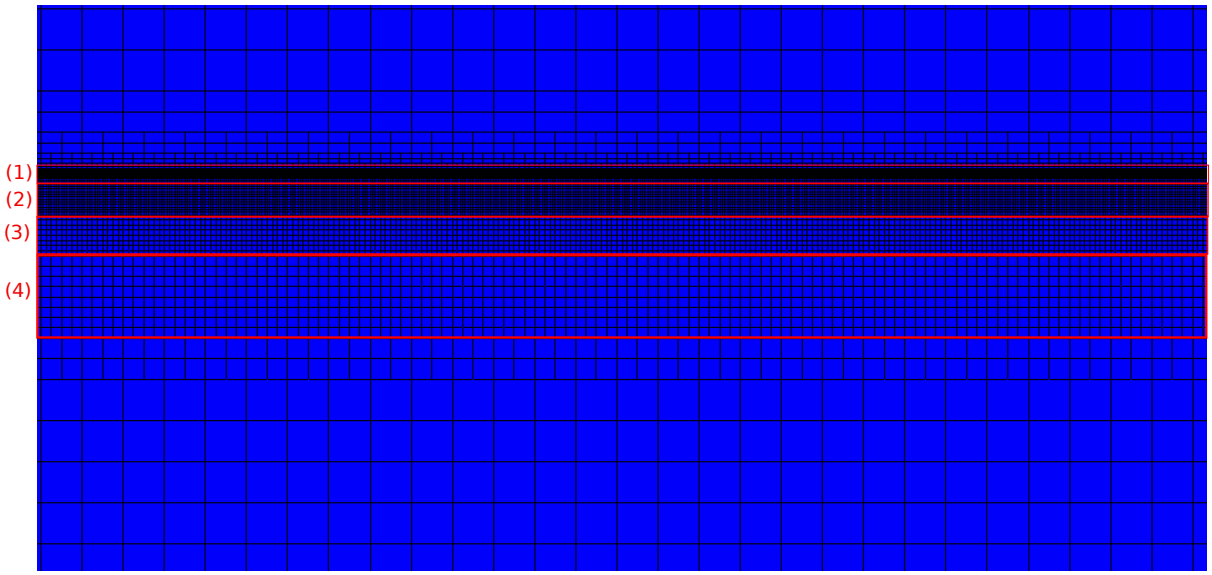

Figure 2.2: Convenient mesh structure for wave propagation; Star-CCM+

Analysis The graphs (Figure (2.3), (2.4), (2.4)) represent the surface elevation along the X axis in the domain. The table(2.3) synthesise the wave damping. "D_{bow}" and "D_{rudder}" are the wave damping at the bow ($x/\lambda = 1.54$) and rudder ($x/\lambda = 0$) of the boat in the related study. "D_{domain}" is the damping at the outlet damping zones limit. The damping zone limits are represented by the dotted lines.

It can be seen that for the "naive" refinement, the damping is about 18.20 percent at the position corresponding to the ship's bow, about 28.5 percent at the stern and up to 46.7 percent before the outlet relaxation zone. This observation stresses the need of refinement box below the free surface using StarCCM+ mesh generator.

On Figure (2.3) and in Table (2.2) it can be seen that the tested vertical refinement below the free surface have a negligible influence on the damping. But adding longitudinal improves a lot the wave propagation. On Figure (2.4) it can be seen that the 4th bow refinement have a negligible impact. And Figure (2.5) highlight the interest of adding fine refinement. Last but not least, for each meshes, foamStar-SWENSE appears to be more accurate than foamStar regarding to the wave propagation.

Those result are consistent regarding to the studies carried out by Li (2018). They also highlight that the small that a quite "coarse" vertical refinement can be applied below the free surface keeping a accurate wave propagation, that benefits the naval application helping to keep a reasonable number of cell in the domain.

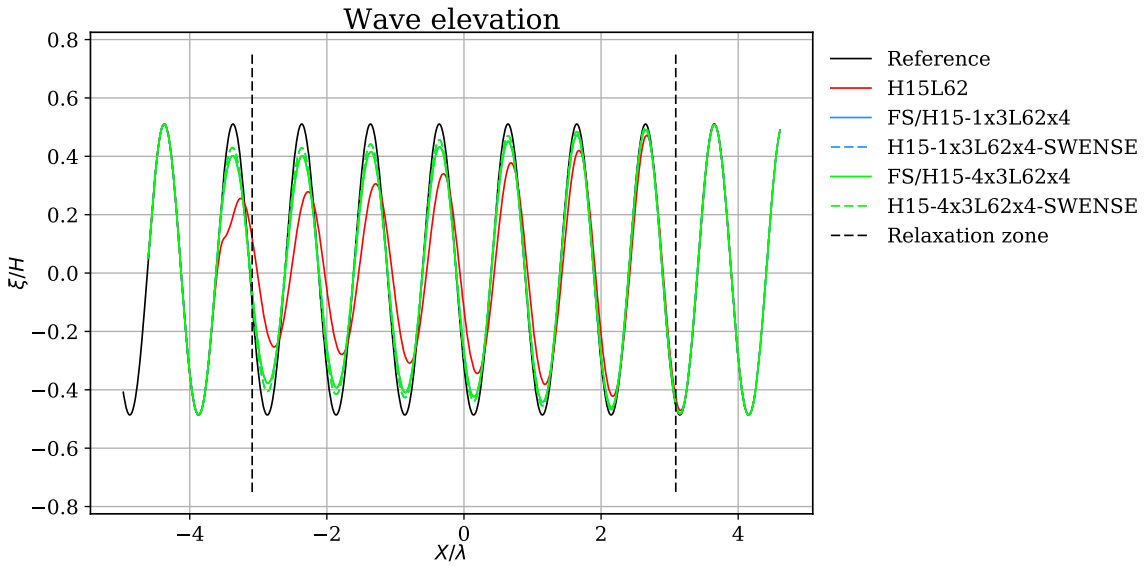

Figure 2.3: Wave damping depending on the mesh refinement (1); λ=3.9 m; ε=0.049; fe/f0=1.81

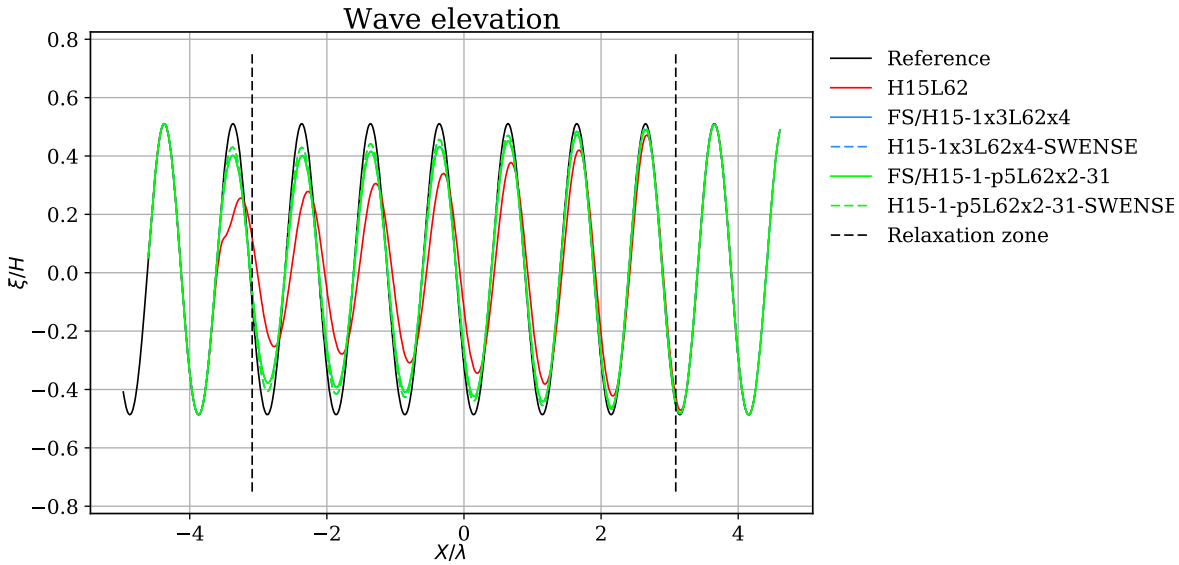

Figure 2.4: Wave damping depending on the mesh refinement (2); λ=3.9 m; ε=0.049; fe/f0=1.81

Table 2.2: 2D mesh refinements

	H15L62 (Naive)		H15-4x3L621x4		H15-1x3L62x4		H15-1-p5L62x2-31		H15-2-1L124x2-62	
Zones	ΔZ	ΔX	ΔZ	ΔX	ΔZ	ΔX	ΔZ	ΔX	ΔZ	ΔX
1	$H/15$	$\lambda/62$	$H/15$	$\lambda/62$	$H/15$	$L/62$	$H/15$	$\lambda/62$	$H/15$	$\lambda/124$
2	x	x	$H/4$	$\lambda/62$	$H/1$	$\lambda/62$	$H/1$	$\lambda/62$	$H/2$	$\lambda/124$
3	x	x	$H/4$	$\lambda/62$	$H/1$	$\lambda/62$	$H/0.5$	$\lambda/31$	$H/1$	$\lambda/62$
4	x	x	$H/4$	$\lambda/62$	$H/1$	$\lambda/62$	x	x	x	x

Table 2.3: Wave damping, 2D case, λ=3.9 m; ε=0.049; fe/f0=1.81

	foamStar			FoamStar-SWENSE		
	D_{bow}	D_{rudder}	D_{domain}	D_{bow}	D_{rudder}	D_{domain}
H15L62 (Naive)	18.20%	28.50%	46.70%			
H15-4x3L62x4	7.70%	12.60%	21.80%	5.35%	9.33%	16.20%
H15-1x3L62x4	7.68%	12.60%	21.70%	5.35%	9.32%	16.20%
H15-1-p5L62x2-31	7.70%	12.60%	21.80%	5.36%	9.34%	16.20%
H15-2-1L124x2-62	3.40%	5.0%	9.57%	1.65%	2.91%	5.50%

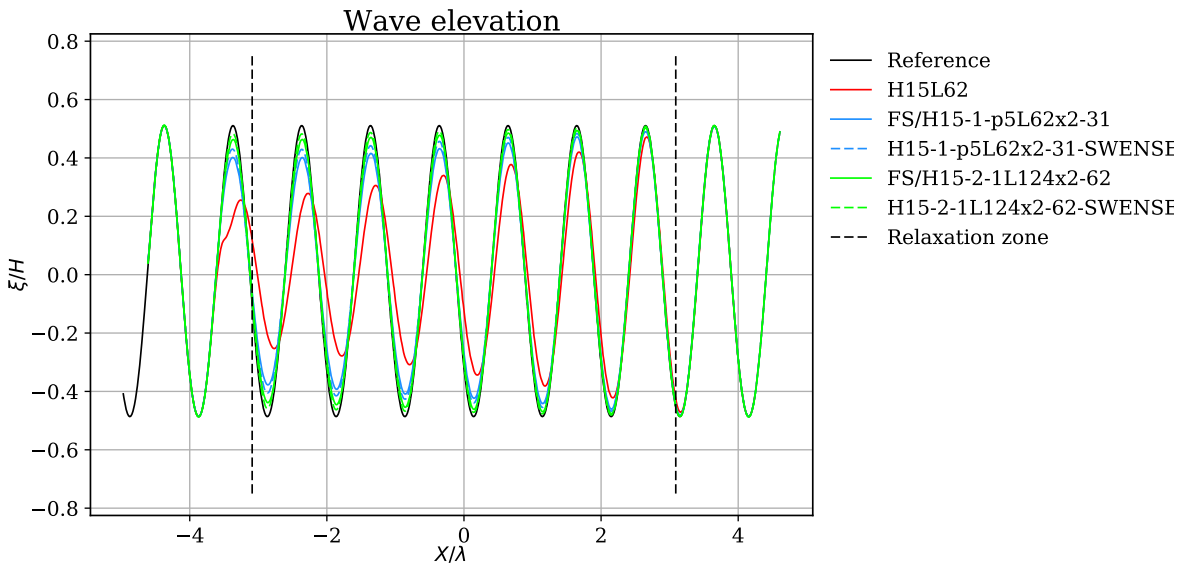

Figure 2.5: Wave damping depending on the mesh refinement (3); λ=3.9 m; ε=0.049; fe/f0=1.81

2.1.2 Irregular waves propagation

The simulation of vessels in irregular wave is one of the principal objective of this Ph.D. Indeed, the previously mentioned HOS method is able to simulate with precision non linear irregular see sates and SWENSE implementation could be an efficient way to use complex irregular sea states (spreading, crossed waves ...) within naval application being as close as possible as real sea states.

Several works have already shown the efficiency of such a method. The next step is to

apply this method on naval application. During the first half of this Ph.D. some studies and developments were done in this direction.

2D

The objective here is not to studied the wave itself but the behaviour of boats in this waves. It might allows some flexibility in term of the sea sate simulation quality. It would be import to test and compare several wave generation method in order to determine the correlation between wave generation accuracy and ship behaviour analysis.

During the first half of this Ph.D., the only work that was done is to take advantage of one of the HOS implementation in order to limit the computation time and the heaviness of the sea state data. Trying to benefit from the spacial periodicity of *HOS-Ocean* solver. Indeed, the *HOS-Ocean* simulation domain is fixed in the earth referential and the CFD domain "moves" inside the HOS domain. The problem with such a method is that simulations with forward speed require the computation of a long HOS domain. In order to limit the size of the HOS domain, small modifications were done in *Grid2Grid* using the *HOS-Ocean* spatial periodicity.

3D

It was expected to test the 3D wave generation provided by HOS in order to simulate vessels in crossed waves. The simulated sea state is composed of two crossed irregular scale model sea states with 10 degrees of spreading. The angle between the two sea states is 45 degrees. HOS was adapted to manage the inputs of two crossed spectrum. It can be seen of figure 2.6 that HOS implementation can now simulate that kind of sea state. The grid shown on the enlarge view represents the modal discretisation. Cases have to be run in order to validate this implementation.

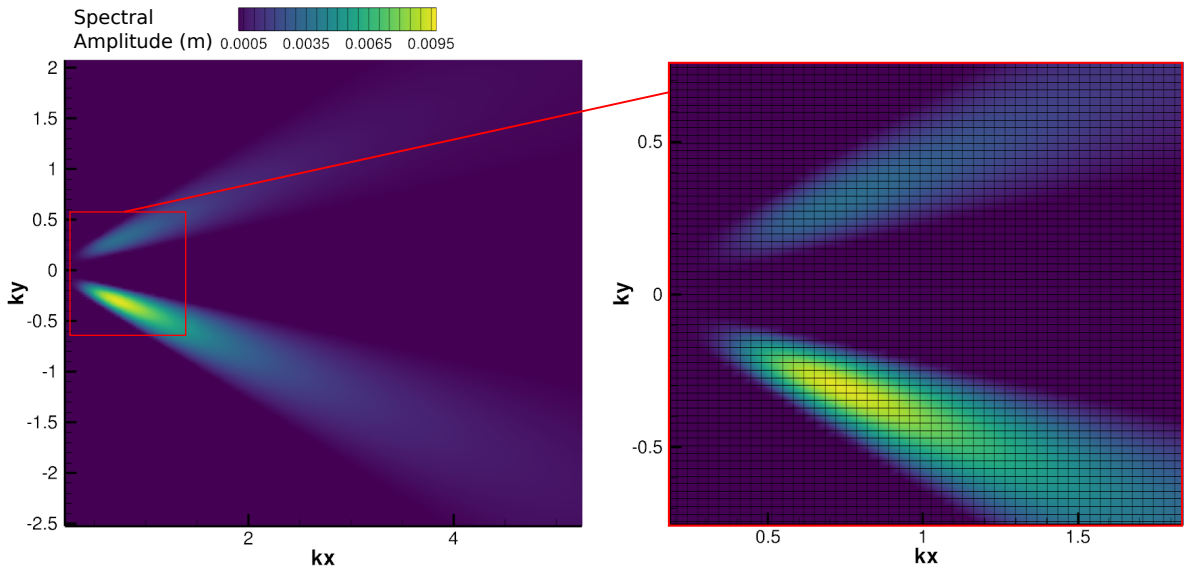

Figure 2.6: HOS-Ocean; crossed irregular waves spectrum; λ=3.9 m; ε=0.049; fe/f0=1.81

2.2 Naval simulations

This section gives an overview of the studies carried out on practical naval application using all the tools previously outlined. In this chapter are also described some specific developments done in order to deal with standard naval applications.

2.2.1 Meshes

Mesh quality As explain in section (1.4.2), distinction between correct mesh refinement and correct cell shapes have to be done. Concerning the first aspect, the convenient refinement for far field and wave propagation was mention in section (2.1.1). The figure (2.7) shows an example of near field and hull refinement used.

The hardest part of mesh generation was to generate valid mesh regarding to the skewness and orthogonality. Many generated meshes result in a simulation crashe. The figure (2.9) is an example of ”wrong mesh” that makes the computation impossible due to the strongly skewed cell identify on the figure. In order to ease the automatic refinement process of the mesh generator it was tried to modify some part of the geometry such as the bow as shown on figure (2.8). In order to control the mesh quality and meet the foamstar expectations, a tools provided by OpenFOAM library called ”checkMesh” analysing the mesh quality is used.

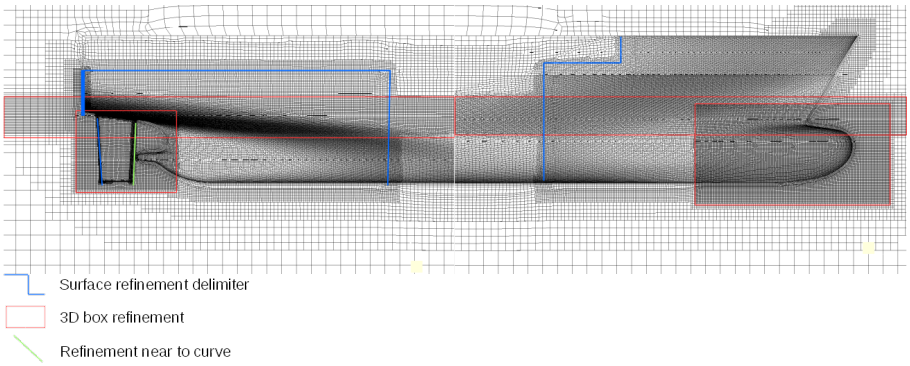

Figure 2.7: KCS mesh zones

Few examples

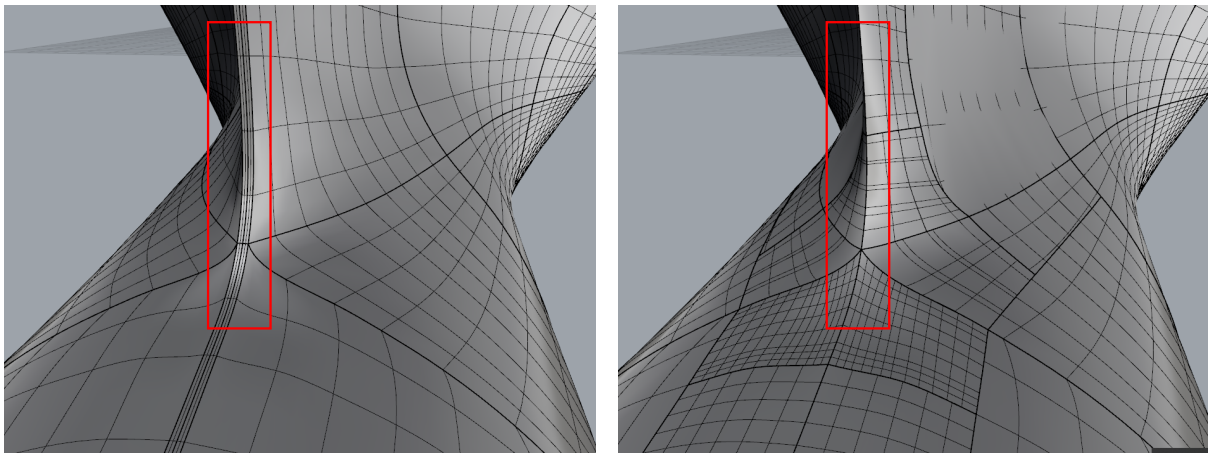

Figure 2.8: Bow correction

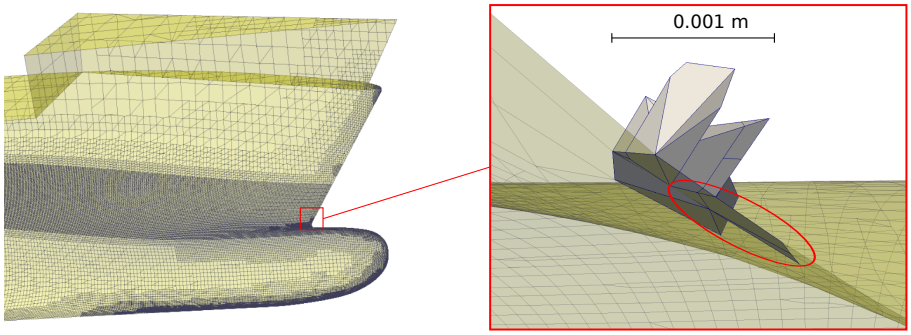

Figure 2.9: Example of bad quality cells at the KCS bow

2.2.2 SWENSE solution

The following study is directly extracted from the submitted paper "Seakeeping in regular and irregular waves with forward speed using a tow-phase functional coupling based SWENSE solver" for the 33rd Symposium on Naval Hydrodynamics.

The objective of the present work is to show the ability of *foamStar-SWENSE* to handle naval seakeeping problems with forward speed for various configurations. To reach this objective, in this study, meshes specifically designed for SWENSE computations have not been considered yet but the algorithm is tested for robustness and accuracy. The numerical analysis are conducted over the Korea Research Institute for Ships and Ocean Engineering (KRISO) Container Ship (KCS). Numerical results obtained with the *foamStar* and *foamStar-SWENSE* solvers are compared to experimental data in regular wave conditions with 3DoF motions and forward speed. A seakeeping simulation in a rough irregular sea state is conducted using *foamStar-SWENSE* in order to highlight the robustness of the solver.

The studied geometry is a scale model (1:37.89) of the KCS. This ship is used in many numerical and experimental investigations of fluid-structure interactions on a modern container ship with a bulbous bow. The KCS model used in this study was provided for the CFD Tokyo 2015 Workshop (Larsson, *et al.*, 2018). The KCS full scale and model scale geometry is summarized in the Table 2.4.

Table 2.4: Main particulars of KCS geometry

Main particulars	Full	Model
Length (L_{PP} [m]	230	6.0702
Breadth (B_{WL}) [m]	32.2	0.8498
Depth (D) [m]	19.0	0.5015
Draft (T) [m]	10.8	0.2850
Volume (Δ) [m^3]	52030	0.9571
Wetted surface (S_W) [m^2]	9539	6.6978
Horizontal buoyancy center (L_{CB}) [m]	111.5	2.944
Vertical Center of Gravity (K_G) [m]	14.32	0.378
Moment of Inertia ($\frac{K_{xx}}{B}$)	0.40	0.40
($\frac{K_{yy}}{L_{PP}}$, $\frac{K_{yy}}{L_{PP}}$)	0.250	0.252

The forward speed condition is presented in Table 2.5 together with the associated non dimensional numbers with the physical parameters in the experimental conditions.

Table 2.5: Physical parameters for KCS experiments and numerical simulations

Ship speed (U_0) [m.s^{-1}]	**Fr**	**Re**
2.017	0.261	$1.074 \cdot 10^7$

In this simulation case, only 2 DoF are considered, the lateral motions being fixed, see Table 2.6.

Table 2.6: Degrees of freedom during KCS experiments and numerical simulations

Surge	**Sway**	**Heave**	**Roll**	**Pitch**	**Yaw**
Towing	*Fixed*	*Free*	*Fixed*	*Free*	*Fixed*

In this study six sea conditions are treated, one in calm water and five with regular head waves. Those conditions are detailed and labelled in Table 2.7 where notations are λ for the wavelengths, H for wave height and $\varepsilon = \mathrm{H}/\lambda$ for the steepness.

Table 2.7: Regular Waves conditions for KCS model scale hull

Case	λ [**m**]	$\frac{\lambda}{\mathbf{L_{PP}}}$	**H** [m]	**T** [s]	ε
C1	3.949	0.651	0.062	1.591	0.016
C2	5.164	0.851	0.078	1.819	0.015
C3	6.979	1.150	0.123	2.115	0.018
C4	8.321	1.371	0.149	2.309	0.018
C5	11.840	1.951	0.196	2.754	0.017

Experimental data relevant to the studied cases were provided for the Tokyo 2015 Workshop that synthesized the towing tank experiments realised by Van et al. (1998), Kim et al. (2001) and updated by Larsson et al. (2013).

Numerical Setup

Figure 2.10 illustrates the computational domain geometry and the boundaries used in the KCS study. The boundary conditions are the specified in Table (**??**).

Table 2.8: Boundary condition, the blue rows represent the variable for SWENSE formulation

	Inlet / Outlet / Side	Body	Air	Bottom
$\mathbf{u}$	$\mathbf{u}_{\text{Incident}}$	$\mathbf{u}_{\text{Wall}}$	Pressure outlet	$\mathbf{u}_{\text{Wall}}$
$\mathbf{u}_{\text{C}}$	Fixed zero vector	$\mathbf{u}_{\text{Wall}} - \mathbf{u}_{\text{Inc}}$	Pressure outlet	Fixed zero vector
p_{d}	Zero gradient	Zero gradient	Fixed value	Fixed value
p_{dC}	Zero gradient	Fixed flux pressure	Fixed value	Fixed value
α	α_{water}	Zero gradient	inlet-outlet	Zero gradient

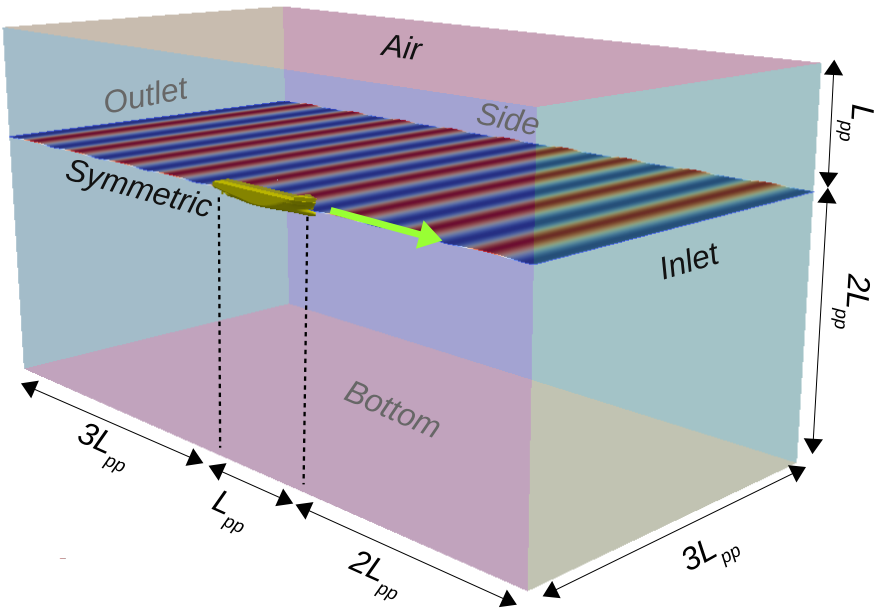

Figure 2.10: Numerical domain for KCS simulations

A set of meshes is generated thanks to the STAR-CCM+® mesh generator and presented in Table 2.9. Each resulting mesh is mainly composed of hexahedral cells, nevertheless, in order to improve the mesh alignment and the viscous layer insertion, any other cell shapes can occasionally be generated. Whatever the case the mesh generation strategy remains the same. Automatic surface refinement is done depending on the curvature of the surface, then a volume mesh is generated and some specific refinements are done near the surface of the hull with denser mesh at the stern. Moreover 3D refinement boxes are added around the bow and at the free surface.

Table 2.9: KCS mesh information

Mesh	$\lambda/\Delta x$	$\lambda/\Delta y$	$H/\Delta z$	Cells	Related case
M1	62	8	16	3.7M	**C1**
M2	82	10	20	3.7M	**C2**
M3	55	14	31	4.3M	**C3**
M4	66	16	19	3.4M	**C4**
M5	47	23	25	3.3M	**C5**
Coarse				2.6M	Calm Water
Medium				3.7M	Calm Water
Fine				5.0M	Calm Water

Various mesh densities were tested in calm water in order to identify an accurate mesh refinement near the body and in the domain except at the free surface where specific refinements are used. The converged results of total resistance (R_T) coefficient $\left(\mathrm{C}_x = 2R_T/(\rho S_w U_0^2)\right)$ on the ship is shown in Table 2.10. It can be seen that the three mesh refinements chosen (labeled "Coarse", "Medium" and "Fine" in Table 2.9) give results with less than 4% of difference with the experiment. As a compromise between accuracy and mesh size, the medium mesh refinement is chosen as a base for the generation of every other mesh used to carry out the rest of the study.

Table 2.10: Calm Water results comparison

	Coarse	Medium	Fine	EFD
$\mathbf{C_x}$	3.973	3.946	3.929	3.835
Err	+3.60%	+2.88%	+2.44%	

The chosen meshes are adapted to each of the five regular wave conditions (Table 2.7). The free surface box refinement is adapted to the wavelengths and wave heights which are considered. An example of resulting mesh is shown on the Figure 2.11 and a synthesis of used meshes is provided in Table 2.9.

The mesh refinement chosen at the free surface is motivated by the studies conducted by Li (2018) and Choi (2019). In order to propagate the waves using as well *foamStar* as *foamStar-SWENSE*, the criterion for the vertical refinement is near to twenty cells per wave height and above fifty cells per wavelength for the longitudinal refinement.

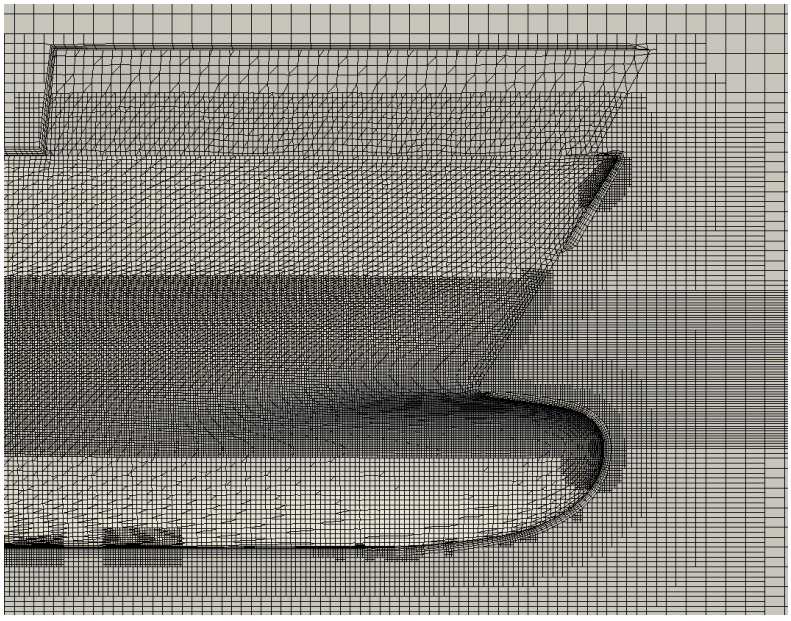

Figure 2.11: Front part of mesh M3 used for the case C3

Numerical results

The experimental data is provided in the form of RAOs computed with the 0th, 1st and 2nd harmonics. To compute the same quantities with the numerical data, a spectral analysis is conducted on the total resistance, surge and pitch time histories for the five wave conditions studied.

The 0th, 1st and 2nd harmonic motion RAOs are presented on Figures 2.12(a), 2.12(b) and 2.13 respectively. The mean heave and pitch obtained with *foamStar* and *foamStar-SWENSE* are similar and follow the experimental data. The first harmonic analysis reveals small differences between the two solvers and the motion responses obtained with the SWENSE method appear to be slightly amplified. *foamStar-SWENSE* is closer to the experimental data close to resonance. This phenomenon might be induced by unwanted damping using the standard wave propagation method in *foamStar*. On Figure 2.13 it can also be seen that also the motion second harmonic amplitudes computed with *foamStar* and *foamStar-SWENSE* are close to each other and follow the experimental data.

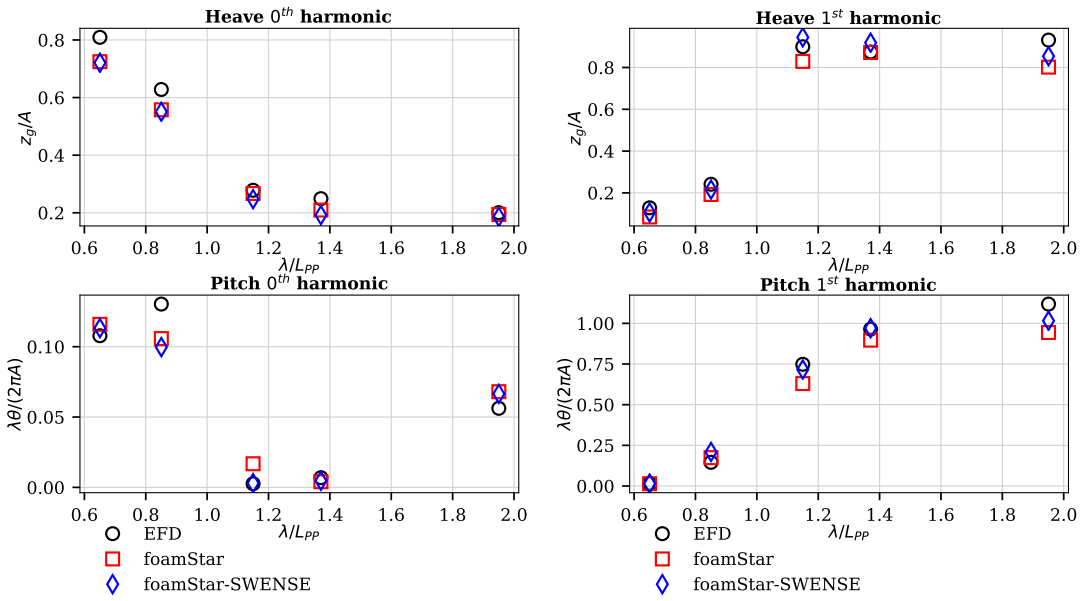

(a) mean

(b) 1st harmonic amplitude

Figure 2.12: KCS front part, meshes comparison between Hexpress and STAR-CCM+

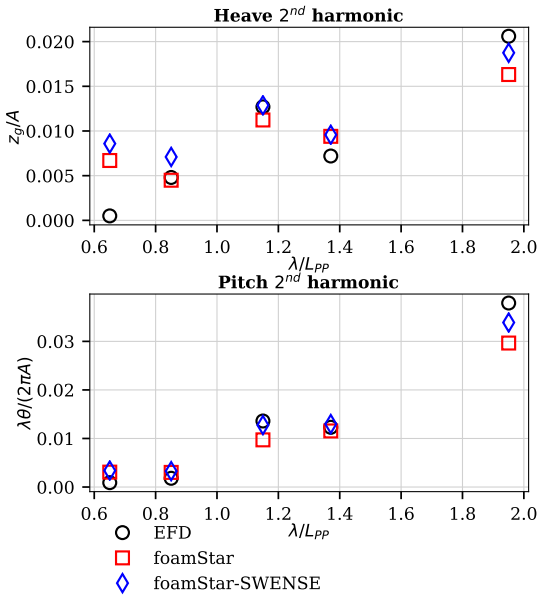

Figure 2.13: KCS heave and pitch 2nd harmonic amplitude, Fr=0.26, head waves

The resistance is also compared with experimental results, as shown with the total and added resistance in Figure 2.14(a).

Total resistance computed with *foamStar* and *foamStar-SWENSE* are close to the experimental results. The added resistance computed with the numerical data are quite different between *foamStar* and *foamStar-SWENSE* for short wavelengths. For those conditions the added resistance magnitude is very small with respect to calm water resistance and the uncertainty on the added resistance computation is high.

Numerical values of the total resistance and differences relative to the experimental data are detailed in Table 2.11 and 2.12 respectively. A similar remark as for the motion analysis can be made concerning the apparent gain of accuracy for total resistance computation near the resonance using SWENSE method.

First and second harmonics for the total resistance are presented in Figure 2.14(b). The first and second harmonic analysis confirms the closeness of the *foamStar* and *foamStar-SWENSE* results and the general agreement with the experiments.

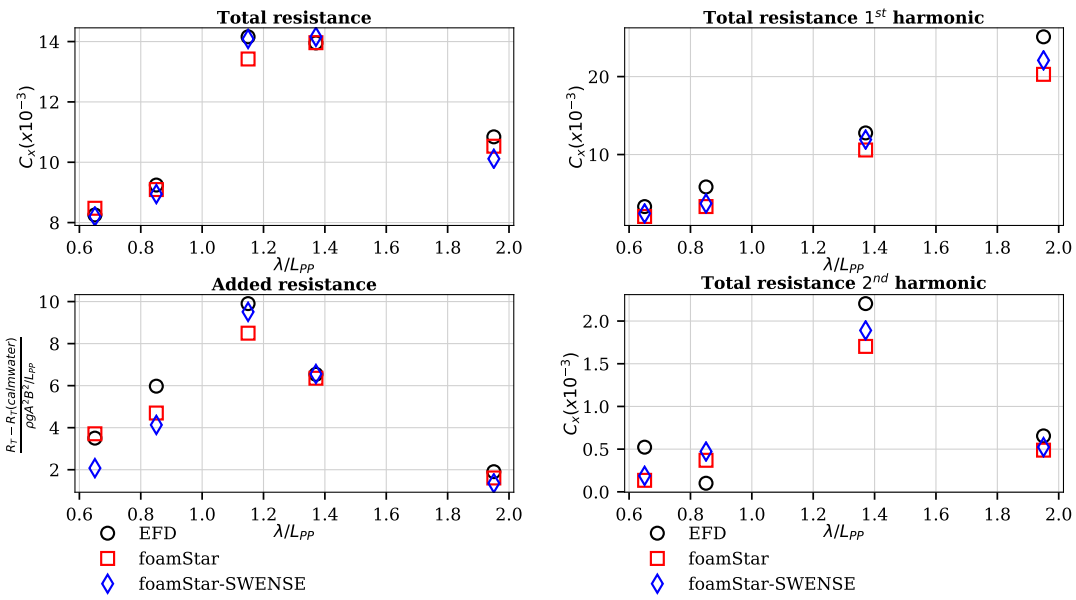

(a) Mean resistance

(b) 1st and 2nd harmonic amplitude

Figure 2.14: KCS total resistance and added resistance, Fr=0.26, head waves

Table 2.11: KCS Total resistance results, (S) exponent stands for *foamStar-SWENSE* and (R) exponent for *foamStar* solver

Case	$C_x^{(EFD)}(10^{-3})$	$C_x^{(S)}(10^{-3})$	$C_x^{(R)}(10^{-3})$
C1	8.25	8.20	8.47
C2	9.24	8.95	9.09
C3	14.16	14.09	13.42
C4	13.96	14.16	13.96
C5	10.84	10.11	10.53

Table 2.12: KCS Total resistance difference with experimental data

Case	$Err^{(S)}$	$Err^{(R)}$
C1	-0.6%	+2.7%
C2	-3.2%	-1.6%
C3	-0.5%	-5.2%
C4	+1.5%	+0.1%
C5	-6.7%	-2.9%

The wave elevation field obtained from *foamStar* and *foamStar-SWENSE* for the C4 condition is presented in Figure 2.15. The wave patterns are globally similar but small differences can be observed, *foamStar-SWENSE* magnitudes being a bit larger.

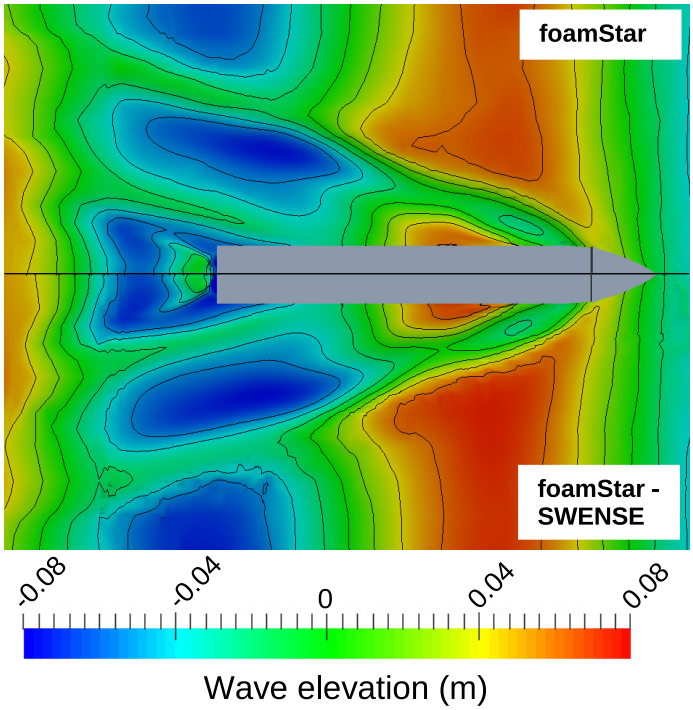

Figure 2.15: Comparison of KCS wake in head wave (C4) using *foamStar* and *foamStar-SWENSE*

KCS in irregular waves

A study of the capability of *foamStar-SWENSE* was carried out on one rough irregular sea sate with forward speed. The chosen sea state is classified with the code six in the World Meteorological Organization. The chosen sea state follows a Pierson-Moskowitz spectrum the characteristics of which are shown in the Table 2.13.

Table 2.13: Irregular sea state (SS6) characteristics

Scale	$\mathbf{H_s}$ [m]	$\mathbf{T_p}$ [s]	$\mathbf{H_s/\lambda_p}$
Full	5.0	12.4	0.021
Model	0.132	2.0145	

The KCS model scale and the mesh generation strategy are the same as for the previous study in regular waves. The free surface refinement is adapted with 33 cells per significant wave height (H_s) and 100 cells per peak wavelength (λ_p). Time step is also adapted so that 500 time steps are computed per encounter peak period ($T_e = 1.23$ s).

This simulation is conducted using the same degrees of freedom and forward speed conditions as for the study in regular waves (Tables 2.5 and 2.6). Figure 2.16 shows the interaction between the wake generated by the ship and the incident waves. Figure

2.17 shows time histories for the heave and pitch responses as well as the total resistance. These preliminary results assess the stability and the ability of the recent *foamStar-SWENSE* implementation to compute such seakeeping problems.

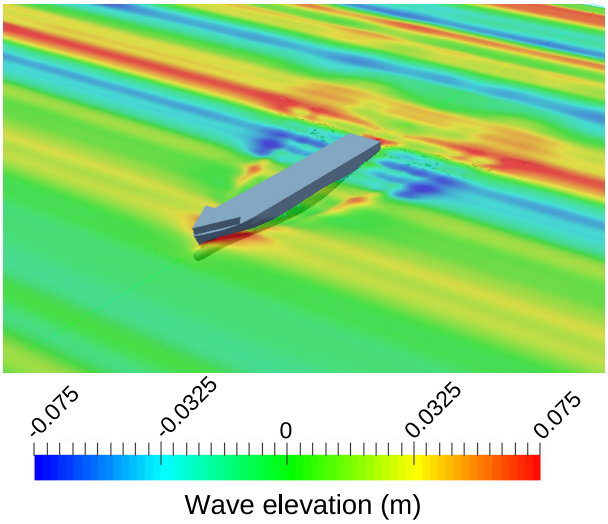

Figure 2.16: KCS wake in irregular head wave (SS6), Fr=0.26

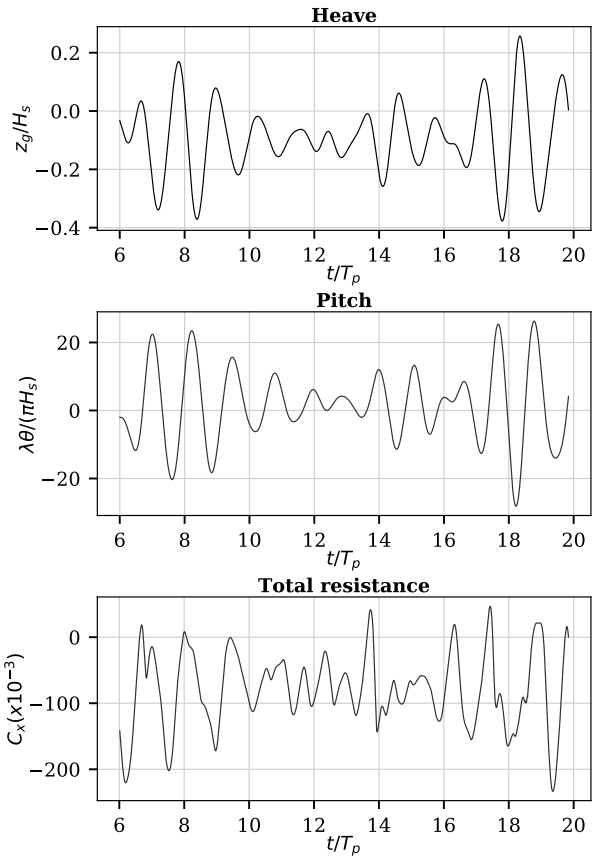

Figure 2.17: KCS motions (heave and pitch) and total resistance response in irregular head wave (SS6), Fr=0.26

SWENSE advantage in allowing the use of less refined meshes in the far-field region

and consequently in reducing the computation time has been already shown in previous studies for cases without forward speed (Li (2018) and Choi (2019)).

This paper presents first results based on recent developments in the *foamStar-SWENSE* solver toward the resolution of naval seakeeping problems with forward speed. These developments appear to be able to reach this objective.

Comparison of results obtained with *foamStar* and *foamStar-SWENSE* on the same meshes does not highlight the capabilities of the SWENSE method but allows to assess its implementation.

It must be verified that the *foamStar-SWENSE* solver is able to keep a good accuracy for lighter meshes in the far-field region. This will be the next step together with further numerical improvements in the implementation of high-order discretisation schemes.

2.2.3 Appendage and manoeuvre

actuator disk

The actuactor disk implementation is in progress. The initial idea was to use the implementation already existing into OpenFOAM library. However, it appeared this implementation did not meet the expectation so a *foamStar* actuator disk was coded. This decision was motivated by the structure of OpenFOAM code that ease the personal implementation of new features based on the existing ones and in the literature it can be found studies about implementation of actuator disk models using OpenFOAM libraries (Svenning).

OpenFOAM OpenFOAM ”actuation disk” implementation is described in the openFOAM user guide OpenFOAM (2006). Two variant of the actuator disk are implemented. The first one is an uniform source distribution integrating two models of force sourcing based on Burton et al. (2011) and van der Laan et al. (2015) work. The second one take into account radial distribution. OpenFOAM implementation seems to match with wind turbine actuator disk models and are inconvenient for naval application because of several reasons:

- the thrust is not coupled with the body motions;
- there is no torque computation;
- the mesh morphing is not taken into account;
- the force sourcing model is based on a ”upstream point” that have to be identify in the simulation domain.

foamStar The actuator disk developed into *foamStar* is for now the simplest version having an interest for industrial project. The model implemented is similar to the ISIS-CFD one (team). The feature of this actuator disk are:

- imposed thrust (thrust adapted to drag is being implemented);
- the actuator disks can be linked to bodies;

- radial force distribution model is used Svenning

The flowchart of the current implementation is shown on Figure (2.18). The adaptative thrust is red-colored because it is not implementated yet. For now no validation cases were done.

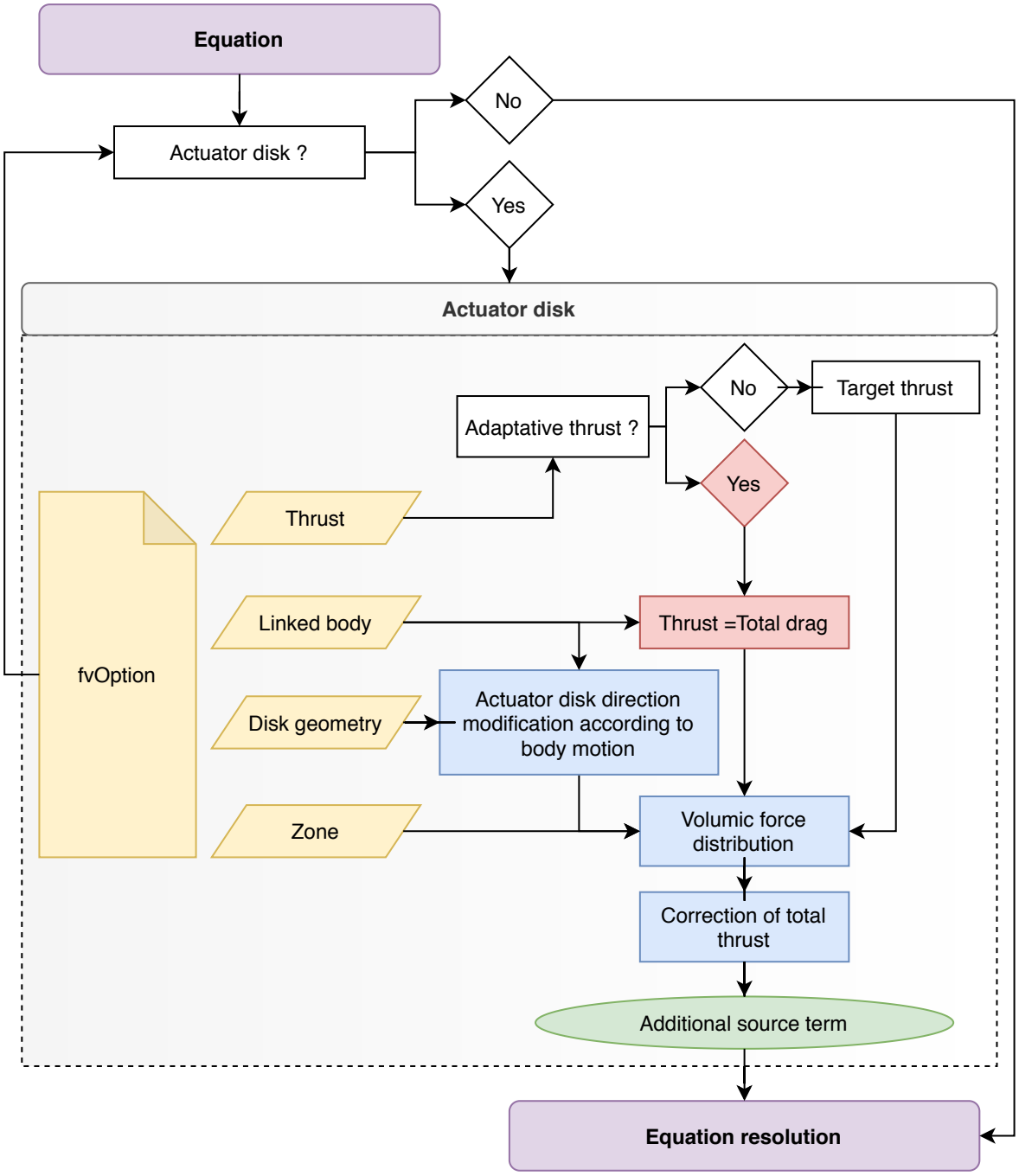

Figure 2.18: *foamStar* actuator disk implementation flowchart

The mathematical model used to compute the radial force distribution is the Goldstein (1929) model. It is the one used by Svenning and ISIS-CFD (team).

Bibliography

R. Beck and A. Reed. Modern seakeeping computations for ships. In *Twenty-Third Symposium on Naval HydrodynamicsOffice of Naval ResearchBassin d'Essais des CarenesNational Research Council*, 2001.

A. Benhamou, S. Seng, C. Monroy, J. de Lauzon, and S. Malenica. Hydroelastic Simulations in OpenFOAM®: A Case Study on a 4400TEU Containership. In *8th International Conference on Hydroelasticity in Marine Technology*, pages 10–12, 2018.

E. Berberović, N. P. Van Hinsberg, S. Jakirlić, I. V. Roisman, and C. Tropea. Drop impact onto a liquid layer of finite thickness: Dynamics of the cavity evolution. *Physical Review E - Statistical, Nonlinear, and Soft Matter Physics*, 79(3), 2009. ISSN 15393755. doi: 10.1103/PhysRevE.79.036306.

T. Burton, N. Jenkins, D. Sharpe, and E. Bossanyi. *Wind Energy Handbook, Second Edition*. 2011. ISBN 9781119992714. doi: 10.1002/9781119992714.

Y. Choi. *Two-way coupling between potential and viscous flows for a marine application*. PhD thesis, École centrale de Nantes, 2019.

Y. Choi, M. Gouin, G. Ducrozet, B. Bouscasse, and P. Ferrant. Grid2Grid: HOS Wrapper Program for CFD solvers. *arXiv preprint arXiv:1801.00026*, 2017.

D. G. Dommermuth and D. K. Yue. A high-order spectral method for the study of nonlinear gravity waves. *Journal of Fluid Mechanics*, 184:267–288, 1987.

G. Ducrozet, F. Bonnefoy, D. Le Touzé, and P. Ferrant. HOS-ocean: Open-source solver for nonlinear waves in open ocean based on High-Order Spectral method. *Computer Physics Communications*, 203:245–254, 2016.

P. Ferrant, L. Gentaz, B. Alessandrini, and D. Le Touzé. A potential/RANSE approach for regular water wave diffraction about 2-D structures. *Ship Technology Research*, 50(4): 165–171, 2003.

J. S. Forrest and I. Owen. An investigation of ship airwakes using detached-eddy simulation. *Computers & Fluids*, 39(4):656–673, 2010.

S. Goldstein. Proceedings of the royal society of london. In *Notes on Numerical Fluid Mechanics and Multidisciplinary Design*, volume 123, pages 440–465. Royal Society, 1929. doi: 10.10098/rspa.1929.0078.

C. W. Hirt and B. D. Nichols. Volume of fluid (VOF) method for the dynamics of free boundaries. *Journal of Computational Physics*, 39(1):201–225, 1981. ISSN 10902716. doi: 10.1016/0021-9991(81)90145-5.

N. G. Jacobsen, D. R. Fuhrman, and J. Fredsøe. A wave generation toolbox for the open-source CFD library: OpenFoam®. *International Journal for Numerical Methods in Fluids*, 70(9): 1073–1088, 2012. ISSN 02712091. doi: 10.1002/fld.2726.

H. Jasak. *Error Analysis and Estimation for the finite volume method with applications to fluid flows*. PhD thesis, Imperial College of Science, Technology and Medicine, 1996a.

H. Jasak. Error analysis and estimation for the finite volume method with applications to fluid flows. 1996b.

W. Kim, D. Van, and D. Kim. Measurement of flows around modern commercial ship models. *Exp. in Fluids*, 31:567–578, 2001.

Y. J. Kim, Y.-M. Choi, B. Bouscasse, Sopheak Seng, and D. Le Touzé. Influence of interface treatment in wave propagation in CFD. In *16èmes Journées de l'Hydrodynamique*, pages 1–10, 2018.

J. Larsen and H. Dancy. Open boundaries in short wave simulations—a new approach. *Coastal Engineering*, 7(3):285–297, 1983.

L. Larsson, F. Stern, and M. Visonneau. *Numerical ship hydrodynamics: an assessment of the Gothenburg 2010 workshop*. Springer, 2013.

L. Larsson, F. Stern, M. Visonneau, T. Hino, N. Hirata, and J. Kim. Tokyo 2015: A workshop on cfd in ship hydrodynamics. In *Workshop Proceedings, Tokyo, Dec*, 2018.

Z. Li. *Two-phase spectral wave explicit Navier-Stokes equations method for wave-structure interactions*. PhD thesis, École centrale de Nantes, 2018.

Z. Li, G. Deng, P. Queutey, B. Bouscasse, G. Ducrozet, L. Gentaz, D. Le Touzé, and P. Ferrant. Comparison of wave modeling methods in CFD solvers for ocean engineering applications. *Ocean Engineering*, 188:106237, 2019. ISSN 00298018. doi: 10.1016/j.oceaneng.2019.106237.

F. Moukalled, L. Mangani, and M. Darwish. *The finite volume method in computational fluid dynamics : An Advanced Introduction with OpenFOAM and Matlab*. Springer International Publishing, 2016. ISBN 9783319168739. doi: 10.1007/978-3-319-16874-6_21.

OpenFOAM. Openfoam: User guide v2006. Technical report, 2006. URL `https://www.openfoam.com/documentation/guides/latest/doc/`.

G. Reliquet, A. Drouet, P. Guillerm, L. Gentaz, and P. Ferrant. Simulation of wave-ship interaction in regular and irregular seas under viscous flow theory using the swense method. In *Proc. 30th Symp. Naval Hydrod.(Tasmania, 11/2014)*, 2014.

M. M. Rienecker and J. D. Fenton. A Fourier approximation method for steady water waves. *Journal of Fluid Mechanics*, 104:119–137, 1981. doi: 10.1017/S0022112081002851.

S. Seng, J. J. Jensen, and Š. Malenica. Global hydroelastic model for springing and whipping based on a free-surface CFD code (OpenFOAM). *International Journal of Naval Architecture and Ocean Engineering*, 6(4):1024–1040, 2014. ISSN 20926790. doi: 10.2478/IJNAOE-2013-0229.

P. R. Spalart. Detached-eddy simulation. *Annual review of fluid mechanics*, 41:181–202, 2009.

E. Svenning. Implementation of an actuator disk inopenfoam. Technical report, Chalmers University of Technology.

M. team. Theory guide, isis-cfd v7.2. Technical report, LHEEA, École centrale de Nantes.

S. Van, W. Kim, G. Yim, D. Kim, and C. Lee. Experimental investigation of the flow characteristics around practical hull forms. *Proceedings 3rd Osaka Colloquium on Advanced CFD Applications to Ship Flow and Hull Form Design, Osaka, Japan*, 1998.

M. P. van der Laan, N. N. Sørensen, P.-E. Réthoré, J. Mann, M. C. Kelly, and N. Troldborg. The k-ε-fp model applied to double wind turbine wakes using different actuator disk force methods. *Wind Energy*, 18(12):2223–2240, 2015. doi: 10.1002/we.1816. URL `https://onlinelibrary.wiley.com/doi/abs/10.1002/we.1816`.

V. Vukčević, H. Jasak, and Š. Malenica. Decomposition model for naval hydrodynamic applications, Part I: Computational method. *Ocean Engineering*, 121:37–46, 2016.

B. J. West, K. A. Brueckner, R. S. Janda, D. M. Milder, and R. L. Milton. A new numerical method for surface hydrodynamics. *Journal of Geophysical Research: Oceans*, 92(C11): 11803–11824, 1987.